

Virial Equation of State and Ideal-Gas Heat Capacities of Pentafluoro-Dimethyl Ether

J. J. Hurly,^{1,2} J. W. Schmidt,¹ and K. A. Gillis¹

Received May 28, 1996

A virial equation of state is presented for vapor-phase pentafluoro-dimethyl ether ($\text{CF}_3\text{-O-CF}_2\text{H}$), a candidate alternative refrigerant known as E125. The equation of state was determined from density measurements performed with a Burnett apparatus and from speed-of-sound measurements performed with an acoustical resonator. The speed-of-sound measurements spanned the ranges $260 \leq T \leq 400$ K and $0.05 \leq P \leq 1.0$ MPa. The Burnett measurements covered the ranges $283 \leq T \leq 373$ K and $0.25 \leq P \leq 5.0$ MPa. The speed-of-sound and Burnett measurements were first analyzed separately to produce two independent virial equations of state. The equation of state from the acoustical measurements reproduced the experimental sound speeds with a fractional RMS deviation of 0.0013%. The equation of state from the Burnett measurements reproduced the experimental pressures with a fractional RMS deviation of 0.012%. Finally, an equation of state was fit to both the speed-of-sound and the Burnett measurements simultaneously. The resulting equation of state reproduced the measured sound speeds with a fractional RMS deviation of 0.0018% and the measured Burnett densities with a fractional RMS deviation of 0.019%.

KEY WORDS: Burnett apparatus; $\text{CF}_3\text{OCF}_2\text{H}$; equation of state; heat capacity; pentafluoro-dimethyl ether; refrigerant; speed of sound; virial coefficient.

1. INTRODUCTION

Ongoing concern over the role of fully halogenated chloro fluorocarbons (CFCs) in the depletion of the earth's protective ozone layer has prompted

¹ Physical and Chemical Properties Division, Chemical Science and Technology Laboratory, National Institute of Standards and Technology, Gaithersburg, Maryland 20899, U.S.A.

² To whom correspondence should be addressed.

the search for alternative refrigerant fluids. The thermodynamic properties, including the equation of state, of each candidate must be determined to evaluate its suitability as a working fluid in thermal machinery. From the wide range of fluids being considered, partially hydrogenated fluor-ethers have emerged as one possible class of replacement refrigerants. As part of this effort, we have measured the vapor-phase density of and the speed of sound in pentafluoro-dimethyl ether ($\text{CF}_3\text{-O-CF}_2\text{H}$), which has been designated E125 by the air-conditioning and refrigeration industry. E125 is a candidate replacement for hexafluoroethane, R116. Figure 1 shows the ranges covered by our vapor-phase measurements, $260 \leq T \leq 400$ K and $0.05 \leq P \leq 5.0$ MPa, and also the vapor pressure curve and the critical point of E125 ($T_c = 354.49$ K and $P_c = 3.3479$ MPa) [1].

Two independent experimental techniques were employed: Burnett density $\rho(P, T)$ measurements and speed-of-sound $u(P, T)$ measurements. The resulting $\rho(P, T)$ and $u(P, T)$ data sets complement one another over the P - T space studied (see Fig. 1). The uncertainties in the Burnett measurements are directly proportional to the uncertainties in the measurement of pressure. These relative uncertainties increase with decreasing pressure. Therefore, the Burnett experiment performs best at high pressures and high to moderate densities. The speed-of-sound apparatus provides highly accurate measurements at low to moderate pressures over a wide temperature range. From the speed of sound one may deduce ideal-gas

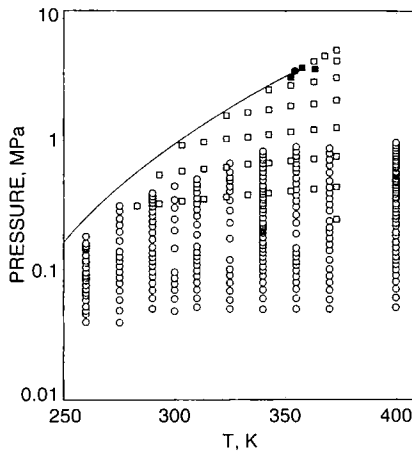


Fig. 1. Location of data. E125's vapor pressure curve and critical point are indicated by the curve and filled circle. \circ , $u(P, T)$; \square , $\rho(P, T)$; \blacksquare , $\rho(P, T)$ points left out of the fit due to their proximity to the critical point.

heat capacities and estimates of the vapor densities [2]. Together, the two apparatuses provide all of the data required to determine the thermodynamic properties of E125 vapor under the conditions encountered in thermal machinery.

The Burnett $\rho(P, T)$ measurements span the ranges $283 \leq T \leq 373$ K and $0.25 \leq P \leq 5.0$ MPa. The $u(P, T)$ measurements cover the ranges $260 \leq T \leq 400$ K and $0.05 \leq P \leq 1.0$ MPa or 80% of the vapor pressure, whichever is less. The $\rho(P, T)$ and $u(P, T)$ data sets were first analyzed separately to determine two independent virial equations of state. The fit to the $\rho(P, T)$ measurements reproduced the Burnett pressures (or densities) with a fractional RMS deviation of 0.012%. The fit to the $u(P, T)$ measurements reproduced the measured speed of sound with a fractional RMS deviation of 0.0013%. A single virial equation of state was then fit to both data sets simultaneously. The resulting function reproduced the measured Burnett pressures (or densities) with a fractional RMS deviation of 0.019% and predicted the measured sound speeds with a fractional RMS deviation of 0.0018%.

2. EXPERIMENTAL TECHNIQUES

2.1. Burnett Measurements

A detailed description of the Burnett apparatus has been given elsewhere [3–5]. Briefly, the heart of the apparatus consisted of two cylindrical chambers with volumes $V_1 \approx 27$ cm³ and $V_2 \approx 18$ cm³. These chambers had been bored out from opposite ends of a solid nickel cylinder. The ratio of the two chamber volumes was accurately determined by a calibration with helium. The sample's pressure was measured relative to a known argon reference pressure by a capacitive-type differential pressure transducer (DPT). The DPT was an integral component of the Burnett cell [6]. The DPT diaphragm formed one end of chamber one and its deflection was sensed capacitively. The reference side of the DPT contained argon gas of a known pressure to balance the sample's pressure within chamber one. The argon pressure was measured with either a quartz Bourdon-type gauge or a deadweight piston gauge. A computer-controlled screw-type piston pump was used to adjust the argon pressure such that the DPT remained in the null condition. The Burnett cell, gas manifold, and transducer spaces were in a thermostated bath whose temperature was stable to within 1 mK. Temperature measurements were made with a standard platinum resistance thermometer and a high-precision multimeter and are reported on ITS-90.

Pressure and temperature measurements were recorded on quasi-isochores between the dew point and the highest temperature (373 K). The volume V_1 was initially loaded to the highest density of ρ_0 at 373 K. After the pressure was measured with both the piston gauge and the Bourdon tube gauge, the valve to the cell was closed. Under computer control, the temperature was lowered to the dew point and then raised in successive steps back up to 373 K. The temperature and pressure were measured at each step. In this automated mode, the pressure was measured with the Bourdon tube gauge only. Once the temperature was returned to 373 K, the pressure was again measured with both the piston and the Bourdon tube gauges. A single Burnett expansion was performed and the pressure measured again. This procedure was repeated until the pressure at 373 K was ~ 250 kPa, at which point uncertainty in the measurement of pressure made further expansions prohibitive.

Nominally, at the beginning and end of an isochore, a single manual measurement of the pressure was made with a deadweight piston gauge referenced to a calibrated barometer. In manual mode, the uncertainty in the pressure measurements was given as $\sigma_p = \sqrt{(44 \times 10^{-6} P)^2 + (10 \text{ Pa})^2}$. All other pressure measurements were performed in the automated mode with a quartz Bourdon tube gauge. The uncertainties associated with the automated measurement of pressure were given by $\sigma_p = \sqrt{(50 \times 10^{-6} P)^2 + (88 \text{ Pa})^2}$.

A correction was made for the thermal expansion of the sample volume V_1 . The density on the j th isochore was related to the density on the 0th isochore at $T_0 = 273.15$ K, through

$$\rho_j(T) = \left(\frac{\rho_0}{N^j} \right) \left(1 + \int_{T_0}^T \alpha(T) dT \right) \quad (1)$$

Here the cell constant from the helium calibration was $N = 1.781327 \pm 0.000035$ and the thermal expansion coefficient $\alpha(T) = [37 + 0.038(T - 273)] \times 10^{-6}$, where α is in K^{-1} and T is in K, was obtained from Ref. 7.

2.2. Speed-of-Sound Measurements

Our laboratory has developed an automated apparatus [8–13] to measure the speed of sound in vapor-phase samples with a high accuracy. This apparatus has been used to study more than 20 gases and gas mixtures [14–21]. A detailed description of the apparatus and the elaborate acoustic model used to reduce the data has been given in previous publications [19, 20]. Briefly, the sample gas was contained in a stainless-steel cylindrical cavity or resonator. The resonator was in a thermostated bath

with millikelvin stability. A 25- Ω capsule-type standard platinum resistance thermometer connected to a high-precision dc multimeter was used to monitor the temperature. All temperatures are reported on ITS-90.

On the top plate of the resonator were two flanges with thin metal diaphragms. The flanges were mounted so that the metal diaphragms were flush with the resonator's interior surface. Exponentially shaped horns functioned as wave guides connecting the diaphragms to remote electro-acoustic transducers in pressurized housings. The diaphragm flanges, waveguides, and transducer housings were filled with argon gas. A quartz Bourdon tube gauge/controller was used to measure and control the argon gas pressure. The pressure gauge had been calibrated with a deadweight piston gauge referenced to a calibrated barometer and was found to have a standard uncertainty of $\sigma_p = \sqrt{(100 \times 10^{-6} P)^2 + (30 \text{ Pa})^2}$. A 13-kPa full-scale differential pressure gauge was used to balance the argon gas pressure in the waveguides and the sample gas pressure within the resonator. The differential pressure gauge and the portion of the manifold in contact with the sample were maintained near 345 K to prevent condensation of the sample at high pressures.

Once the sample was loaded in the resonator and the pressure across the metal diaphragms was balanced, the speed of sound in the sample could be measured. The source transducer acted as a speaker generating sound. The sound was transmitted through the waveguide and the thin metal diaphragm into the sample. Sound within the sample was coupled through the second diaphragm and up the second waveguide to the detector transducer. The resonance frequencies were determined by varying the frequency of the source transducer using well-established procedures [9, 17–19]. The resonance frequencies were combined with the dimensions of the cylinder and the acoustical model [19, 20] to yield the speed of sound in the sample. The dimensions of the resonator were determined by measuring the resonance frequencies in argon, a gas for which the sound speed is accurately known. This calibration accounted for the temperature dependence of the dimensions.

The speed-of-sound measurements were taken on isotherms by first loading the resonator to 1 MPa or 80% of the sample's vapor pressure. The temperature and pressure were allowed to equilibrate, and the resonance frequencies were determined. The pressure was then reduced in successive steps by collecting the sample in a trap cooled to 77 K. After each pressure change, the temperature and pressure were allowed to equilibrate, and the resonance frequencies of several modes were measured. This process was repeated down to a pressure of approximately 50 kPa, where the decrease in the signal-to-noise ratio prevented further measurements.

3. SAMPLE COMPOSITION

A gas chromatograph (GC) was used to analyze the composition of the E125 sample: as received, after the Burnett measurements, and then again after the speed-of-sound measurements. Impurities were detected and subsequently identified by GC mass spectroscopy. The post-Burnett analysis identified four species within the sample with the following area fractions: 0.0207% N_2 , 0.0058% CHF_3 , 0.0373% H_2O , and a balance of 99.94% $\text{CF}_3\text{OCF}_2\text{H}$. The post-speed-of-sound analysis showed only three species: 0.0069% CHF_3 , 0.0321% H_2O , and a balance of 99.96% $\text{CF}_3\text{OCF}_2\text{H}$. The post-speed-of-sound analysis showed that the nitrogen had been removed. This change in composition was explained by the sample preparation technique used in the acoustical measurements. After the sample bottle was connected to the speed-of-sound apparatus' manifold, but prior to loading the resonator, the sample was frozen at 77 K with liquid nitrogen, and the remaining volatile gases were removed. This process was repeated until the residual pressure above the sample at 77 K was less than 0.1 Pa. Species within the sample with significant vapor pressures at 77 K such as O_2 and N_2 but not H_2O or CF_3H were removed during this process, as is confirmed by the post-speed-of-sound analysis.

The ideal-gas heat capacities deduced from speed-of-sound measurements are very sensitive to sample composition. The square of the speed of sound is inversely proportional to the average molecular weight of the sample. The uncertainty in the molecular weight of the sample is related to the uncertainties of the concentrations of the impurities. For E125, the uncertainty in $C_p^{\circ}(T)$ as deduced from speed-of-sound data is approximately 12 times the uncertainty in the average molecular weight. The E125 sample was treated as though it were pure because it was found that the experimental uncertainties were an order of magnitude greater than the uncertainties due to composition. For example, the 300 K isotherm independently yielded an ideal-gas heat capacity $C_p^{\circ}/R = 12.640 \pm 0.014$, while the correction for the known impurities was $+0.0013R$, an order of magnitude smaller than the uncertainty in C_p°/R .

A concern was the possible thermal decomposition of the E125 sample at the higher temperatures. The speed of sound in E125 was repeatedly measured for more than 2 h at 400 K and 100 kPa. During this 2-h period, the speed of sound in the sample did not vary by more than the experimental uncertainty under these conditions, $\pm 0.001\%$, showing that the average molecular weight of the sample did not change. Two other facts support this conclusion. The duplicate 400 K isotherms reproduced each other within the experimental uncertainties and no increase was observed in the concentration of CHF_3 in the postexperiment analysis of the sample.

4. RESULTS

4.1. Burnett $\rho(P, T)$ Measurements

Vapor-phase $\rho(P, T)$ measurements were made along seven isochores. These results are presented in Table II. In all, 72 points were taken covering the ranges $283 \leq T \leq 373$ K and $0.25 \leq P \leq 5.0$ MPa. The higher-accuracy pressure measurements taken with the deadweight piston gauge are indicated in Table II.

4.2. Speed-of-Sound Measurements

The speed of sound in E125 was measured at 268 points along 13 isotherms between 260 and 400 K. Initially four resonance modes were examined: two longitudinal, (3, 0, 0) and (4, 0, 0); and two radial, (0, 0, 1)

Table I. Parameters for Virial Equation of State

	$\rho(P, T)$	$u(P, T)$	$\rho(P, T)$ and $u(P, T)$
$C_p^o R$			
A_0	—	4.2781e+00	6.3478e+00
A_1 (K ⁻¹)	—	2.7078e-02	7.9444e-03
A_2 (K ⁻²)	—	1.4000e-05	7.2998e-05
A_3 (K ⁻³)	—	-3.5282e-08	-9.5496e-08
$B(T)$ (m ³ ·mol ⁻¹)			
b_0 (m ³ ·mol ⁻¹)	1.5732e-04	1.3226e-04	1.3495e-04
λ	1.3185	1.3095	1.3164
ε (K)	420.1160	459.4790	448.5419
$C(T)$ (m ³ ·mol ⁻¹) ²			
b_0 (m ³ ·mol ⁻¹)	2.6973e-04	3.0263e-04	2.4535e-04
λ	1.1331	1.1210	1.2067
ε (K)	577.6256	567.4973	464.2512
$D(T)$ (m ³ ·mol ⁻¹) ³			
b_0 (m ³ ·mol ⁻¹)	9.4115e-05	1.4484e-04	7.9154e-05
λ	2	2	2
ε (K)	155.9463	169.9628	107.5444
$E(T)$ (m ³ ·mol ⁻¹) ⁴			
E_0 (m ¹² ·mol ⁻⁴)	1.2015e-14	—	8.2804e-15
E_1 (m ¹² ·mol ⁻⁴ ·K)	-9.1833e-12	—	-6.3242e-12
E_2 (m ¹² ·mol ⁻⁴ ·K ²)	1.7197e-09	—	1.1838e-09
Fitting statistics			
χ^2	137	137	991
df	58	256	322
χ^2/df	2.38	0.54	3.08

Table II. E125 Burnett $\rho(P, T)$ Measurements

T (K)	P (kPa)	ρ ($10^3 \text{m}^3 \cdot \text{mol}^{-1}$)
358.12	3618.67 ^h	4.51365
368.17	4422.18	4.51181
373.13	4824.85	4.51090
373.13	4825.01	4.51090
363.17	4018.87	4.51273
373.12	4824.34	4.51090
373.12	4824.23 ^u	4.51090
373.12	4824.31	4.51090
373.12	3995.14 ^u	2.53233
353.16	3196.24 ^h	2.53438
363.17	3605.37 ^h	2.53335
373.16	3996.65	2.53232
373.16	3996.55 ^u	2.53232
373.16	3996.55	2.53232
373.15	2996.67 ^u	1.42159
373.15	2996.74	1.42159
343.14	2428.68	1.42332
353.15	2624.39	1.42275
363.15	2813.04	1.42217
373.17	2996.96	1.42159
373.17	2997.02 ^u	1.42159
373.17	2997.08	1.42159
373.15	1994.88 ^u	0.79805
373.15	1994.86	0.79805
323.64	1540.67	0.79963
333.09	1632.40	0.79934
343.14	1726.34	0.79902
353.13	1817.43	0.79870
363.15	1906.73	0.79838
373.16	1994.58	0.79805
373.15	1994.86 ^u	0.79805
373.15	1994.88	0.79805
373.15	1232.11 ^u	0.44801
373.15	1232.07	0.44801
303.11	910.04	0.44925
313.15	959.00	0.44908
323.17	1006.58	0.44891

Table II. (Continued)

T (K)	P (kPa)	ρ ($10^3 \text{m}^3 \cdot \text{mol}^{-1}$)
333.10	1052.65	0.44873
343.13	1098.38	0.44855
353.13	1143.40	0.44837
363.14	1187.87	0.44819
373.16	1231.90	0.44801
373.16	1232.18 ^a	0.44801
373.16	1232.19	0.44801
373.15	729.50 ^a	0.25150
373.15	729.49	0.25150
293.16	539.79	0.25230
303.12	564.45	0.25220
313.15	588.91	0.25210
323.12	612.83	0.25201
333.11	636.63	0.25191
343.15	660.18	0.25181
353.14	683.37	0.25171
363.14	706.43	0.25161
373.16	729.32	0.25150
373.16	729.56	0.25150
373.14	729.56 ^a	0.25150
373.15	421.85 ^a	0.14119
373.15	421.81	0.14119
283.15	308.01	0.14169
293.16	321.03	0.14163
303.11	333.93	0.14158
313.15	346.82	0.14153
323.18	359.53	0.14147
333.11	372.12	0.14142
343.15	384.70	0.14136
353.14	397.12	0.14130
363.14	409.54	0.14125
373.16	421.88	0.14119
373.15	421.91 ^a	0.14119
373.15	421.90	0.14119
373.16	240.71	0.07926

^a Manual piston gauge measurement.^b Data left out of fit.

Table III. E125 Speed-of-Sound Measurements

P (kPa)	u ($\text{m} \cdot \text{s}^{-1}$)	$\sigma[u]/u$ (ppm)
$T = 399.97 \text{ K}$		
888.96	153.613	28
846.56	154.016	13
806.05	154.401	12
767.18	154.770	15
730.47	155.118	19
674.42	155.647	17
642.38	155.947	16
592.81	156.413	17
547.72	156.833	1
505.27	157.227	2
481.33	157.450	2
438.03	157.851	4
404.96	158.156	13
368.95	158.488	21
336.23	158.789	28
306.85	159.057	44
268.61	159.409	36
231.77	159.745	48
194.79	160.084	44
164.86	160.356	44
140.33	160.580	36
134.05	160.636	42
122.66	160.740	46
112.47	160.832	44
100.82	160.937	42
92.58	161.014	41
82.05	161.110	28
72.14	161.201	31
$T = 399.94 \text{ K}$		
934.51	153.173	41
890.66	153.592	49
822.45	154.241	38
783.71	154.608	27
723.98	155.173	31
669.49	155.689	41
612.20	156.224	18
559.90	156.713	11
512.76	157.152	6
469.76	157.550	5
429.18	157.926	12
397.35	158.220	24

Table III. (Continued)

P (kPa)	u ($\text{m} \cdot \text{s}^{-1}$)	$\sigma[u]/u$ (ppm)
363.73	158.530	25
324.16	158.894	36
289.78	159.212	19
256.37	159.515	40
225.14	159.802	36
187.21	160.147	42
152.04	160.466	54
141.84	160.560	32
132.46	160.644	43
122.45	160.735	46
113.39	160.817	42
101.42	160.926	40
92.41	161.009	39
82.18	161.103	24
61.76	161.291	5
51.44	161.383	28
$T = 369.98 \text{ K}$		
867.11	145.363	2
807.18	146.136	10
717.63	147.275	15
655.24	148.061	14
562.37	149.217	5
485.38	150.165	10
441.63	150.699	8
400.18	151.201	5
362.48	151.656	7
328.42	152.066	6
288.76	152.539	17
242.30	153.091	14
216.88	153.389	38
199.85	153.591	31
178.96	153.836	34
160.14	154.056	45
143.46	154.252	34
120.73	154.518	40
101.49	154.742	42
90.87	154.867	23
81.46	154.977	21
70.64	155.103	12
59.80	155.230	2
50.79	155.335	1

Table III. (Continued)

P (kPa)	u ($\text{m} \cdot \text{s}^{-1}$)	$\sigma[u]/u$ (ppm)
$T = 354.98 \text{ K}$		
915.18	139.924	2
891.99	140.281	4
851.10	140.906	6
780.72	141.971	2
754.43	142.364	0
722.41	142.840	0
672.73	143.574	2
626.86	144.245	2
583.81	144.869	1
537.51	145.535	7
514.53	145.863	5
472.19	146.464	7
433.45	147.011	14
387.34	147.657	18
346.21	148.228	21
314.18	148.668	18
268.50	149.294	15
234.59	149.754	8
191.68	150.333	5
151.65	150.869	1
141.38	151.006	2
132.05	151.130	5
121.60	151.271	6
112.14	151.395	3
101.20	151.540	4
91.45	151.670	4
81.51	151.797	10
72.14	151.920	3
61.18	152.066	0
51.01	152.201	3
$T = 339.98 \text{ K}$		
847.44	135.876	30
820.13	136.371	36
768.50	137.298	31
738.53	137.829	16
692.08	138.646	21
648.36	139.405	22
600.24	140.229	2
560.81	140.897	3
518.78	141.602	9

Table III. (Continued)

P (kPa)	u ($\text{m} \cdot \text{s}^{-1}$)	$\sigma[u]/u$ (ppm)
466.00	142.474	10
447.19	142.784	22
428.81	143.085	21
411.49	143.367	23
384.40	143.806	27
368.65	144.060	30
344.04	144.454	32
329.87	144.680	33
307.75	145.032	34
286.40	145.369	38
261.27	145.765	40
243.04	146.050	42
233.14	146.203	61
223.48	146.356	31
214.25	146.498	42
205.42	146.635	42
191.25	146.854	44
183.37	146.975	51
170.79	147.169	42
163.76	147.278	41
152.57	147.449	43
142.32	147.606	44
132.64	147.755	30
121.66	147.921	38
111.66	148.073	39
102.50	148.212	39
91.80	148.375	37
80.74	148.543	21
71.14	148.689	9
60.70	148.846	0
50.30	149.002	18
50.30	149.004	16
$T = 324.99 \text{ K}$		
658.33	134.273	23
587.58	135.725	20
522.48	137.027	11
499.84	137.474	7
454.13	138.365	0
427.79	138.872	6
410.49	139.202	17
347.74	140.385	34

Table III. (Continued)

P (kPa)	u ($\text{m} \cdot \text{s}^{-1}$)	$\sigma[u]/u$ (ppm)
293.65	141.388	34
234.28	142.473	26
178.86	143.464	43
122.71	144.455	40
102.65	144.804	48
92.35	144.986	23
82.53	145.156	19
70.62	145.364	3
60.64	145.537	2
50.57	145.714	16
$T = 309.99 \text{ K}$		
508.31	132.448	61
482.09	133.066	58
449.63	133.820	38
410.40	134.719	42
374.51	135.527	35
336.73	136.364	20
303.40	137.093	14
264.33	137.935	19
227.16	138.722	6
191.54	139.467	9
154.16	140.240	9
144.32	140.441	13
133.87	140.655	9
123.08	140.873	13
112.64	141.087	7
102.32	141.296	13
92.35	141.496	10
82.11	141.700	1
72.03	141.902	7
62.34	142.096	25
53.45	142.272	13
$T = 299.99 \text{ K}$		
444.97	130.608	33
352.92	132.966	22
308.21	134.071	18
251.91	135.430	16
205.13	136.532	19
150.27	137.797	34
98.98	138.951	31

Table III. (Continued)

P (kPa)	u ($\text{m} \cdot \text{s}^{-1}$)	$\sigma[u]/u$ (ppm)
89.31	139.166	40
80.31	139.364	24
72.25	139.542	34
61.25	139.784	33
49.66	140.038	38
417.68	127.857	32
390.28	128.665	37
369.59	129.264	20
345.52	129.951	7
322.50	130.599	9
297.44	131.295	3
274.50	131.922	2
249.77	132.589	1
225.88	133.225	4
201.72	133.859	6
178.64	134.457	7
153.56	135.099	7
143.96	135.343	3
134.06	135.592	10
123.42	135.860	4
112.74	136.127	0
101.98	136.395	16
92.46	136.630	9
81.97	136.890	22
71.48	137.148	35
61.76	137.384	35
52.12	137.619	58
$T = 275.00 \text{ K}$		
321.47	125.551	1
293.78	126.499	19
259.03	127.658	35
231.82	128.541	32
204.29	129.417	27
174.09	130.357	27
143.47	131.289	13
133.91	131.577	21
122.48	131.918	18
111.97	132.229	14
102.67	132.502	12
92.44	132.803	32
82.40	133.094	22

Table III. (Continued)

P (kPa)	u ($\text{m} \cdot \text{s}^{-1}$)	$\sigma[u]_{ju}$ (ppm)
71.06	133.421	18
61.06	133.710	36
51.00	133.997	43
41.09	134.280	66
$T = 260.02 \text{ K}$		
188.40	125.267	16
172.21	125.882	18
157.27	126.441	3
138.59	127.126	20
122.32	127.716	1
111.75	128.094	5
102.21	128.432	3
91.76	128.799	21
82.39	129.126	30
71.62	129.499	38
60.76	129.870	36
51.24	130.195	58
41.23	130.530	71
$T = 260.00 \text{ K}$		
164.24	126.171	6
152.58	126.605	2
137.87	127.144	3
126.27	127.565	10
112.20	128.069	13
101.99	128.431	15
96.01	128.641	28
88.53	128.903	30
81.72	129.141	38
75.52	129.354	42
68.25	129.605	43
61.75	129.827	41
54.95	130.059	50
48.00	130.295	56

and (0, 0, 2). All four modes provided the same speed of sound within $\pm 0.005\%$. Mode (3, 0, 0) was at a frequency that had excessive noise, and mode (0, 0, 2) had a weak signal at low pressures. Thus, modes (4, 0, 0) and (0, 0, 1) were measured for each pressure along each isotherm. The speed-of-sound measurements presented in Table III are the averages of the two modes weighted by the standard deviation of their fit to the individual resonances. In Table III $\sigma[u]/u$ is the estimated fractional uncertainty in u in parts per million. $\sigma[u]/u$ was obtained from a weighted average of the uncertainties of the two resonance frequency measurements. This uncertainty was used as a weight when fitting the $u(P, T)$ surface. The isotherms at 260 K and 400 K were repeated.

5. ANALYSIS

Both the $u(P, T)$ and the $\rho(P, T)$ experimental results were independently analyzed to provide a density virial equation of state:

$$P = RT\rho[1 + B(T)\rho + C(T)\rho^2 + D(T)\rho^3 + E(T)\rho^4 + \dots] \quad (2)$$

For the speed-of-sound measurements, the density series was truncated after the fourth virial coefficient $D(T)$, and for the Burnett measurements, the density series was truncated after the fifth virial coefficient $E(T)$. A single virial equation of state truncated after $E(T)$ was then fit to both data sets simultaneously. The temperature dependences of $B(T)$, $C(T)$, and $D(T)$ were assumed to be those of the hard-core square-well potential model [2], where the algebraic expressions are given as

$$B(T) = b_0[1 - (\lambda^3 - 1)\Delta] \quad (3)$$

$$C(T) = \frac{1}{8}b_0^2(5 - c_1\Delta - c_2\Delta^2 - c_3\Delta^3) \quad (4)$$

$$c_1 = \lambda^6 - 18\lambda^4 + 32\lambda^3 - 15$$

$$c_2 = 2\lambda^6 - 36\lambda^4 + 32\lambda^3 + 18\lambda^2 - 16$$

$$c_3 = 6\lambda^6 - 18\lambda^4 + 18\lambda^2 - 6$$

$$D(T) = b_0^3(0.2869 + 1.634\Delta - 23.29\Delta^2 + 54.65\Delta^3 + 70.76\Delta^4 - 168.2\Delta^5 - 12.74\Delta^6) \quad (5)$$

where $\Delta = e^{\varepsilon/k_B T} - 1$, and k_B is Boltzmann's constant. The adjustable parameters are ε , the well depth; λ , the ratio of the width of the well to the diameter σ of the hard core; and the molar volume of the hard core, $b_0 = 2/3\pi N_A \sigma^3$, where N_A is Avogadro's constant. The algebraic expression

for $D(T)$ is known only for certain values of λ and Eq. (5) is that when $\lambda \equiv 2.0$. The temperature dependence of $E(T)$ was expressed as a polynomial-inversely proportional to temperature.

$$E(T) = E_0 + \frac{E_1}{T} + \frac{E_2}{T^2} \quad (6)$$

5.1. Burnett $\rho(P, T)$ Alone

Equation (2) was fit directly to the Burnett $\rho(P, T)$ data using Eqs. (3)–(6) by a nonlinear fitting algorithm developed by one of us (K.A.G.). When comparing the densities calculated from the equation of state from the experimental densities, three points were found to have deviations well in excess of three standard deviations. These points were measured close to the critical point (see Fig. 1) and were omitted from the regression because the virial equation of state is not suitable for the critical region. The final fit had 58 degrees of freedom (df), with a $\chi^2 = 138$ and a resulting χ^2/df of 2.38. The resulting parameters are presented in Table I. The resulting equation of state reproduced the $\rho(P, T)$ experimental pressures with a fractional RMS deviation of 0.012%. Figure 2 shows the differences of the measured pressures from those calculated with the present equation of state.

5.2. Speed of Sound $u(P, T)$ Alone

The speed-of-sound in a dilute vapor can be expressed as a series in terms of pressure P such that

$$u^2 = \left(\frac{\gamma^\circ(T) RT}{m} \right) \left(1 + \frac{\beta_a(T)}{RT} P + \frac{\gamma_a(T)}{RT} P^2 + \frac{\delta_a(T)}{RT} P^3 + \frac{\varepsilon_a(T)}{RT} P^4 + \dots \right) \quad (7)$$

Here $\gamma^\circ(T) = C_p^\circ(T)/(C_v^\circ(T) - R)$, R is the gas constant, $m = 0.136020$ kg/mol is the molar mass, and $\beta_a(T)$, $\gamma_a(T)$, $\delta_a(T)$, and $\varepsilon_a(T)$, are the second, third, fourth, and fifth acoustic virial coefficients, respectively. The acoustic virial coefficients are related to the density virial coefficients $B(T)$, $C(T)$, $D(T)$, $E(T)$, and γ° by [2]

$$\beta_a = 2B + 2(\gamma^\circ - 1) B_1 + [(\gamma^\circ - 1)^2/\gamma^\circ] B_{11} \quad (8a)$$

$$\gamma_a = (L - \beta_a B)/(RT) \quad (8b)$$

$$\delta_a = (M - \beta_a C - 2RT\gamma_a B)/(RT)^2 \quad (8c)$$

$$\varepsilon_a = [N + \beta_a(2BC - D) - B(RT\gamma_a B + 3(RT)^2 \delta_a)]/(RT)^3 \quad (8d)$$

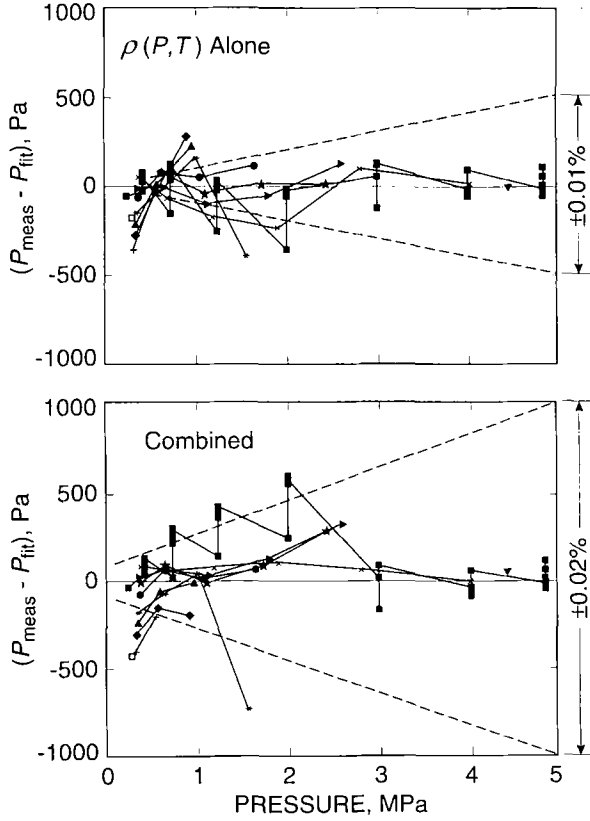


Fig. 2. Deviation plot of $\rho(P, T)$ data from (top) the fit to only $\rho(P, T)$ data and (bottom) the simultaneous fit to both $\rho(P, T)$ and $u(P, T)$ data. ■, 373 K; ▼, 368 K; ×, 363 K; ►, 353 K; ★, 343 K; ●, 333 K; *, 323 K; ▲, 313 K; ◆, 303 K; +, 293 K; □, 283 K.

where

$$L = \frac{(\gamma^o - 1)}{\gamma^o} Q^2 + \frac{(2\gamma^o + 1)}{\gamma^o} C + \frac{(\gamma^{o2} - 1)}{\gamma^o} C_i + \frac{(\gamma^o - 1)^2}{2\gamma^o} C_{ii} \quad (9)$$

$$M = \frac{(\gamma^o - 1)^2}{\gamma^o} Q^2(2B_i + B_{ii}) + \frac{(\gamma^o - 1)}{\gamma^o} QP + \frac{2(\gamma^o + 1)}{\gamma^o} D + \frac{2(\gamma^o - 1)(\gamma^o + 2)}{3\gamma^o} D_i + \frac{(\gamma^o - 1)^2}{3\gamma^o} D_{ii} \quad (10)$$

$$\begin{aligned}
N = & \frac{(\gamma^{\circ} - 1)^3}{\gamma^{\circ}} Q^2 (2B_I + B_{II})^2 B_{II} + \frac{2(\gamma^{\circ} - 1)^2}{\gamma^{\circ}} Q (2B_I + B_{II})(C + C_I) \\
& + \frac{(\gamma^{\circ} - 1)^2}{2\gamma^{\circ}} Q [B + (6\gamma^{\circ} - 5) B_I + 3(\gamma^{\circ} - 1) B_{II}] (2C_I + C_{II}) \\
& + \frac{(\gamma^{\circ} - 1)^2}{4\gamma^{\circ}} P^2 + \frac{2(\gamma^{\circ} - 1)^2}{3\gamma^{\circ}} Q [3D + (2\gamma^{\circ} - 1) D_I + (\gamma^{\circ} - 1) D_{II}] \\
& + \frac{(2\gamma^{\circ} + 3)}{\gamma^{\circ}} E + \frac{(\gamma^{\circ} - 1)(\gamma^{\circ} + 3)}{2\gamma^{\circ}} E_I + \frac{(\gamma^{\circ} - 1)^2}{4\gamma^{\circ}} E_{II} \quad (11)
\end{aligned}$$

with $P = 2C + 2\gamma^{\circ}C_I + (\gamma^{\circ} - 1)C_{II}$, and $Q = B + (2\gamma^{\circ} - 1)B_I + (\gamma^{\circ} - 1)B_{II}$. Here we have introduced the notation $A_I \equiv T(dA/dT)$ and $A_{II} \equiv T^2(d^2A/dT^2)$. The constant-pressure ideal-gas heat capacity was fit to a polynomial expansion in temperature,

$$\frac{C_P^{\circ}}{R} = A_0 + A_1 T + A_2 T^2 + A_3 T^3 \quad (12)$$

Equations (7)–(12) allow the speed of sound to be calculated directly from the density virial equation of state and, inversely, allow us to determine the density virial coefficients by fitting Eq. (1) to our speed-of-sound measurements. The comparatively limited pressure range of the speed-of-sound measurements required only three terms in the density virial equation of state. [Note that in Eq. (8) the expression for ε_n contains contributions from the lower-order density virials and therefore is not zero when only three density virials are considered.] The $u(P, T)$ measurements were fit to Eq. (1) using a nonlinear regression algorithm incorporating Eqs. (7)–(12). The parameters from this regression are given in Table I. Twelve parameters were varied: four defined $C_p^{\circ}(T)$, three each defined $B(T)$ and $C(T)$, and two defined $D(T)$ because λ was fixed at the value of 2. Figure 3 shows the fractional deviations of the measured sound speeds from those calculated from the present equation of state and ideal-gas heat capacities. The fit had a $\chi^2 = 137$, with 256 df, giving a $\chi^2/(df) = 0.54$. The resulting equation of state reproduced the speed-of-sound data for E125 with a fractional RMS deviation of 0.0013%.

5.3. Simultaneous Fit of $\rho(P, T)$ and $u(P, T)$

A single virial equation of state was simultaneously fit to both $\rho(P, T)$ and $u(P, T)$ data sets. As before, the temperature dependence of $B(T)$, $C(T)$, and $D(T)$ were taken as that of the square-well potential model. $E(T)$ was expressed as a three-term inverse polynomial expansion of T , and

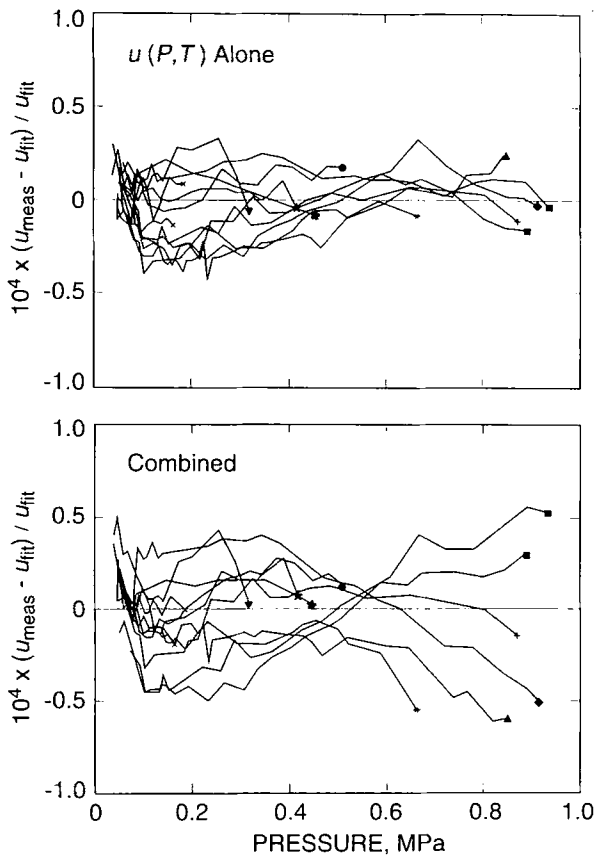


Fig. 3. Fractional deviations of $u(P, T)$ from the equations of state determined from (top) the fit to $u(P, T)$ alone and (bottom) the simultaneous fit to both $u(P, T)$ and $\rho(P, T)$ data. ■, 400 K; +, 370 K; ◆, 355 K; ▲, 340 K; *, 325 K; *, 300 K; ●, 310 K; ★, 290 K; ▼, 275 K; ×, 260 K.

$C_p^o(T)$ was fit to a four-term polynomial expansion of T . Initially the parameters for $C_p^o(T)$ were fixed at those determined by the fit to $u(P, T)$ alone, however, a significant reduction in χ^2 was observed once they were allowed to vary. The resulting parameters for the simultaneous fit are given in Table I. The fit had a $\chi^2 = 991$, with 322 df, giving a $\chi^2/(df) = 3.08$. The equation of state from the simultaneous fit reproduced the measured speed of sound in E125 with a fractional RMS deviation of 0.0018% and the Burnett $\rho(P, T)$ measurements with a fractional RMS deviation of 0.019%. Figures 2 and 3 show, respectively, the differences and the deviations of

the $\rho(P, T)$ and $u(P, T)$ measurements from the values calculated with the present equation of state. This single equation of state's ability to reproduce both data sets over the extensive $P\rho T$ space studied (Fig. 1) comments favorably on the accuracy and precision of our experimental results.

6. CONCLUSIONS

Gillis and Moldover [2] examined the use of the square-well potential to model the temperature dependence of the virial coefficients deduced from $u(P, T)$ data. They found that in the region where the reduced temperature (T/T_c , where T_c is the critical temperature) is of the order of one, the square-well model provides a superior fit to the inverse T polynomial expansion. They also showed how the use of the square-well model allowed a reasonable extrapolation beyond the measured temperature range. Gillis and Moldover found that in the worst case, the vapor density deduced from $u(P, T)$ differed from the independent measurements by the remarkably small value of 0.07%. Here, the temperature range spanned by the E125 $u(P, T)$ and $\rho(P, T)$ data corresponds to $0.073 \lesssim T/T_c \lesssim 1.13$, where $T_c = 354.49$ K [1]. We have employed the same model and procedures as Gillis and Moldover and thus were not surprised by the high degree of agreement between the present $\rho(P, T)$ and $u(P, T)$ data sets.

ACKNOWLEDGMENT

This research was supported in part by the Environmental Protection Agency.

REFERENCES

1. J. W. Schmidt, E. Carrillo-Nara, and M. R. Moldover, submitted for publication.
2. K. A. Gillis and M. R. Moldover, *Int. J. Thermophys.* **17**:1305 (1996).
3. M. Waxman and J. R. Hastings, *J. Res. Natl. Bur. Stand.* **75C**:165 (1971).
4. D. Linsky, J. M. H. Levelt Sengers, and H. A. Davis, *Rev. Sci. Instrum.* **58**:817 (1987).
5. D. Linsky, J. M. H. Levelt Sengers, and J. S. Gallagher, *Fluid Phase Equil.* **36**:149 (1987).
6. M. Waxman and W. T. Chen, *J. Res. Natl. Bur. Stand.* **69C**:27 (1964).
7. D. E. Gray (ed.), *The American Institute of Physics Handbook*, 3rd ed. (McGraw-Hill, New York, 1972), pp. 4-126.
8. M. R. Moldover, M. Waxman, and M. Greenspan, *High Temp. High Press.* **11**:75 (1979).
9. J. B. Mehl and M. R. Moldover, *J. Chem. Phys.* **74**:4062 (1981).
10. J. B. Mehl and M. R. Moldover, in *Proc. 8th Symp. Thermophys. Prop.*, J. V. Sengers, ed. (Am. Soc. Mech. Eng., New York, 1982), pp. 134-141.
11. M. R. Moldover, J. B. Mehl, and M. Greenspan, *J. Acoust. Soc. Am.* **79**:253 (1986).

12. M. R. Moldover, J. P. M. Trusler, T. J. Edwards, J. B. Mehl and R. S. Davis, *J. Res. Natl. Bur. Stand.* **93**:85 (1988).
13. J. P. M. Trusler, *Physical Acoustics and Metrology of Fluids* (Adam Hilger, Bristol, 1991).
14. A. R. H. Goodwin and M. R. Moldover, *J. Chem. Phys.* **93**:2741 (1990).
15. A. R. H. Goodwin and M. R. Moldover, *J. Chem. Phys.* **95**:5230 (1991).
16. A. R. H. Goodwin and M. R. Moldover, *J. Chem. Phys.* **95**:5236 (1991).
17. K. A. Gillis and M. R. Moldover, in *Proceedings of the 9th Symposium on Energy Engineering Sciences* (Argonne National Laboratory, May 13-15, 1991), p. 310.
18. D. Delibaugh, K. A. Gillis, M. R. Moldover, G. Morrison, and J. W. Schmidt, *Fluid Phase Equil.* **81**:285 (1992).
19. K. A. Gillis, *Int. J. Thermophys.* **15**:821 (1994).
20. K. A. Gillis, A. R. H. Goodwin, and M. R. Moldover, *Rev. Sci. Instrum.* **62**:2213 (1991).
21. K. A. Gillis, *Int. J. Thermophys.* **18**:73 (1996).